MEASUREMENT OF LATERAL DIFFUSION IN LIPIDS

by

Andrey V. Tataurov

Diploma, Electrical Engineering, Mari State University, 2000

Submitted to the Graduate Faculty of

The University of Pittsburgh in partial fulfillment

of the requirements for the degree of

Master of Science

University of Pittsburgh

2005

UNIVERSITY OF PITTSBURGH

FACULTY OF ARTS AND SCIENCES

This thesis was presented

by

Andrey V. Tataurov

It was defended on

April 19, 2005

and approved by

Stephane Petoud

Shigeru Amemiya

Sunil Saxena
Thesis Advisor

MEASUREMENT OF LATERAL DIFFUSION IN LIPIDS

Andrey V. Tataurov, M.S.

University of Pittsburgh, 2005

Different techniques to study lateral diffusion of lipids are reviewed, including long-range diffusion methods and short-range diffusion methods. Long-range diffusion methods require the measurements of the time needed to fill a given area of the membrane. Applications of fluorescence recovery after photobleaching (FRAP) method are discussed. Short-range diffusion methods measure the rate of bimolecular collisions. The methods include fluorescence quenching, fluorescence energy transfer, nuclear magnetic resonance and electron spin resonance spectroscopy. Special attention is given to Electron Spin Resonance (ESR) spectroscopy. Procedure of obtaining diffusion coefficient *D* using novel two dimensional electron double-double resonance experiment (2D-ELDOR) is discussed in greater detail. In order to demonstrate the feasibility of using 2D Fourier Transform ESR spectroscopy for lateral diffusion studies, the *D* of spin-labeled phospholipids sample is estimated by 2D-ELDOR method.

TABLE OF CONTENTS

LIST OF TABLES

LIST OF FIGURES

1.0 INTRODUCTION

Biological membranes have been the center of much recent research in biochemistry and biophysics, principally because of the important role they play in cellular phenomena. Assemblies of lipids and protein molecules form biological membranes. One of the main features of these highly organized systems is the lack of covalent linkages between lipids and proteins which allow these molecules to have conformational, rotational and translational motions [1].

One hypothesis for the structure of the cell membrane is the Fluid Mosaic Model [2]. This model proposed that membranes are two-dimensional solutions of oriented lipids and proteins that are highly dynamic in nature (Figure 1). As a result, both lipid molecules and proteins must be randomly distributed within the membrane and the lipid phase has a bulk physical property, for instance fluidity.

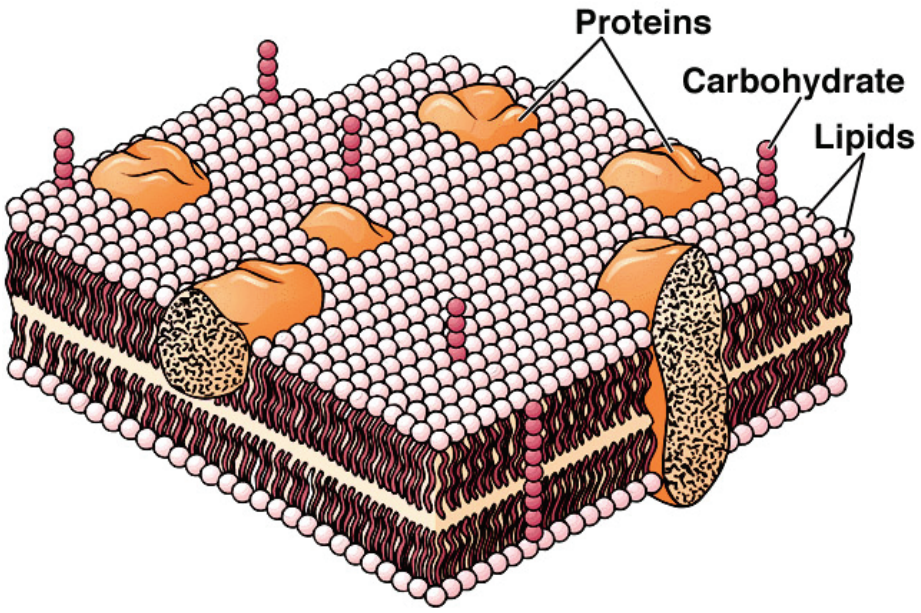

Figure 1 Illustration of a Fluid Mosaic Model [3]

Lipids are fatty acid esters, a class of relatively water-insoluble organic molecules, which are the main components of biological membranes. Lipids consist of a polar or hydrophilic head and one to three nonpolar hydrophobic tails. There are three major classes of lipid molecules: phospholipids, glycolipids, and cholesterol [4]. One of the main lipid components of most biological membranes is phospholipids, which can have a variety of headgroups and acyl chains. When put in water, at a critical concentration phospholipids spontaneously aggregate to form bilayer structures, and the interactions between different bilayers result in a thermodynamically stable multilamellar structure.

An important, if not essential, characteristic of a membrane is lateral diffusion of lipid molecules, diffusion in the plane of a membrane. The diffusion coefficients, D of *E. coli* lipids are about 10^{-8}-10^{-7} cm^2s^{-1} [4].

The connection between the lateral organization of the membranes and their functions can be understood by studying the lateral diffusion of the lipids and proteins. Different membrane parameters can be controlled by the lateral motion of lipids. For instance, Venable *et al* proposed that there is an intimate connection between the microviscosity of the headgroup region and upper hydrophobic part of the phospholipids and the lateral diffusion rate [5].

Biological membranes are compressible structures and comprise pockets of "free volume" (holes). The free volume fraction estimates a volume that is accessible to a small molecule in the membrane. Solute molecules permeating the membrane can occupy these pockets. Another hypothesis is that the rate of the lateral diffusion controls the fluctuations of the free volume, and thus translational mobility of the lipids is closely connected to the permeability of small molecules across the membrane. One argument that supports this hypothesis is that the water permeability across eukaryotic lipids is proposed to depend on the lateral diffusion rates of

lipids [6]. Essentially, studying lateral diffusion in lipids might help one to understand the mechanism of membrane permeation and hence provide important information about membrane functionality.

This document will focus on the lateral diffusion of lipids in membranes. We will discuss first different techniques which can be used to determine the diffusion coefficient *D*, mentioning the difference between short-range and long-range diffusion. Then, we will introduce the concepts of how two-dimensional Electron-Electron Double Resonance [7, 8] (2D-ELDOR) can be used to obtain translational rates in lipids.

2.0 METHODS FOR OBTAINING THE DIFFUSION COEFFICIENT OF LIPIDS

There are two main categories for determining the diffusion coefficient *D* of lipids:

1. Long-range diffusion measurements: *D* is obtained from the time required to fill out a given area of the membrane. An example of this approach is Fluorescence Recovery After Photobleaching (FRAP) technique.
2. Short-range diffusion measurements: Diffusion coefficients are measured from the frequencies of bimolecular collisions within the membrane using Nuclear Magnetic Resonance (NMR), ESR, and fluorescence spectroscopy.

The diffusion coefficient, *D* is measured over different lengthscale using above mentioned techniques. For instance, *D* is estimated over a long distance (few microns) in FRAP experiments, while in collisional techniques (ESR, fluorescence quenching etc.), *D* is estimated over short distances (few nanometers). The *D* values determined by different approaches are rather different as well. There is no direct explanation to this discrepancy. As a matter of fact, a given lipid membrane system should have only one value of *D*, and this value cannot be dependent of the method of investigation.

We will present the method from the first category because of its significant contribution to the *D* measurements. However, we will discuss mainly methods from the second category, mentioning their corresponding advantages and disadvantages.

2.1 LONG-RANGE DIFFUSION MEASUREMENTS

2.1.1 Fluorescence spectroscopy

The emission properties of a fluorescent molecule depend upon molecular conformation and dynamics. Hence, the structure and dynamics of a given region of a membrane can be monitored by measurement of emission parameters when such a molecule is placed into that particular region of a membrane. The important experiment parameters are the fluorescence spectrum, fluorescence efficiency, excitation spectrum, lifetime, and degree of polarization of emitted light [9].

An Energy level diagram can provide the best explanation of the emission and absorption properties of a fluorophore (fluorescent substance), as demonstrated in Figure 2 [10, 11].

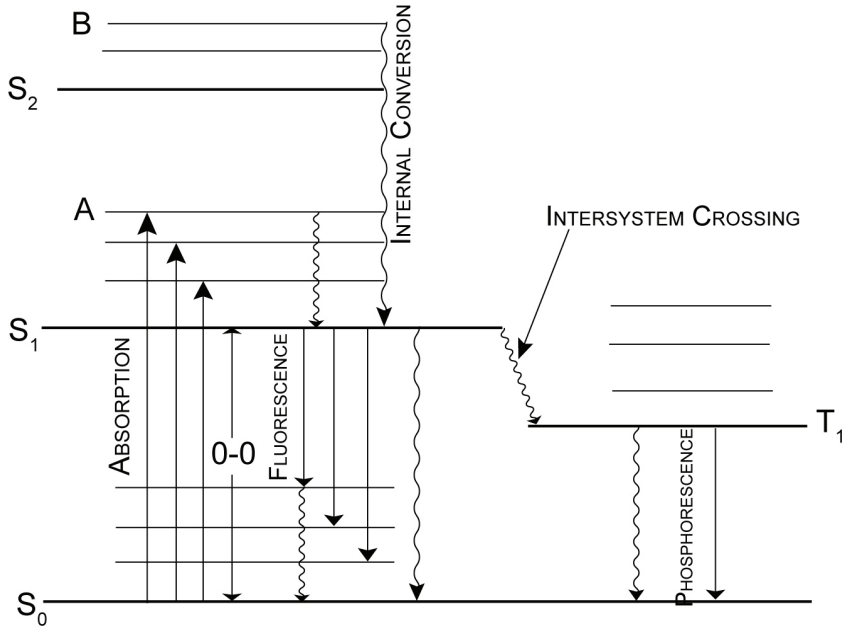

Figure 2 Energy Level Diagram of a fluorophore. Light absorbing or emitting processes are represented by straight arrows, nonradiative processes are shown as wiggly arrows. S_0 is the ground singlet electronic state; S_1 and S_2 are the first and second electronically excited states. T_1 is the first triplet state

Electronic energy levels are illustrated by long horizontal lines. An electron can be excited (elevated) into high orbitals. Several vibrational levels are possible within each electronic state, and they are illustrated by the shorter horizontal lines. Moreover, for every vibrational level several rotational levels are possible, but since they have very small energy gap these are not shown.

Under normal conditions, virtually all molecules of the fluorophore are in the lowest possible electronic and vibrational energy level (the Boltzman Distribution case), which is called the ground electronic-vibrational energy state, or the ground state. When light of a wavelength λ is applied on a solution of fluorophore, the molecules will absorb energy from the light source if the energy of a photon $h\nu$ is equal to the energy difference between the ground state and one of the higher energy states. By scanning continuously the wavelength of the incident light, one can obtain the excitation spectrum.

One feature of a fluorescence spectrum is that emission of light is possible only from the zero vibrational level of S_1 (see Figure 2). Excited fluorophore molecules located in the upper levels (e.g. A or B in Figure 2) fall down (time < 10^{-10} s) quickly to the level S_1 without emission of radiation. The emission spectrum can show vibrational structure or be continuous [9]. Since a fluorophore has a single radiative state, there is only one emission spectrum for a particular homogeneous solvent, and it is independent of λ of incident light. The emission spectrum is always located at longer wavelengths than the absorption spectrum. Figure 2 demonstrates that absorption vertical lines are longer than the shorter emission lines (smaller energy, longer wavelengths).

It is worth stressing that not every excited fluorophore molecule emits light. That occurs since there is always a competition between nonradiative and radiative processes. The portion of fluorophore molecules which emit light is termed the fluorescence efficiency or quantum yield.

2.1.2 Fluorescence Recovery After Photobleaching

One of the essential techniques, based on the phenomenon of fluorescence to measure lateral motion in the plane of the membrane, is Fluorescence Recovery after Photobleaching (FRAP) method [12, 13]. Using this method, the membrane component is labeled with a fluorophore. A small region of the membrane is then illuminated by a weak beam of incident light and fluorescence is recorded. Then, fluorescent molecules in this region are destroyed by the intense pulse from a laser (molecules are photochemically changed into a permanently nonfluorescent form). After the bleaching pulse, the fluorescence of this region is constantly detected as a function of time. At first, the fluorescence intensity is low, but it increases with time since new fluorescent labeled molecules move from unbleached areas into the bleached area. Thus, lateral mobility can be estimated from the rate of recovery of fluorescence intensity [14].

Poo and Cone first studied the lateral diffusion of membrane components by monitoring lateral diffusion of rhodopsin in the photoreceptor membrane using microspectrophotometric observations [15]. Axelrod devised the first FRAP apparatus in 1976 [16]. A simple set-up consists of a fluorescence microscope paired with a laser beam for illumination.

The diffusion coefficient can be calculated using the following formula [16]

$$D = \left(\frac{r^2}{4\tau_{1/2}} \right) \gamma_D \tag{1}$$

where r is the radius of the excitation spot, $\tau_{1/2}$ is the half-recovery time, determined from the experimental fluorescence intensity plot, γ_D is the bleaching parameter. For a laser beam with circular excitation profile γ_D=0.88. For a laser beam of Gaussian intensity profile γ_D can be determined from the empirical plot (p.1062 of [16]).

Significant advantage of FRAP is that this technique is applicable to living intact cells. In most cases, FRAP experiments are performed on single cells within a given cell population and an important problem is first to calculate diffusion coefficient correctly for each cell, and then it is necessary to analyze the distribution of this value over the whole cell population [1].

There is a variety of lipophilic (having an affinity for lipids) fluorescent probes that can be used in FRAP experiments. The most widely used fluorophores are anthracene, oxa- and indo-carbocyanine, fluoresscein, rhodamine, and nitrobenzoxadiazole. There are two general classes: the fatty acid and the phospholipids-like molecules in which the various fluorescent groups are attached either to the polar or to the nonpolar region of the probe molecules, monitoring on different zones of the lipid bilayer. An example of a probe that is located near the membrane interface with water is fluorescein [17], which can interact with integral and peripheral membrane proteins. On the contrary, nitrobenzoxadiazole derivatives can be attached to a given carbon atom along acyl chain [18] and report information from hydrophobic core of a membrane.

It is important to realize that when we use the probe approach, two requirements must be satisfied. First, the amount of probe molecules introduced into the plasma membrane should be less than a few mol % and is usually 1-5 mol % of the all membrane phospholipids. By exceeding this limit, one can obtain significant perturbation of the membrane structure. In addition, the fluorescence intensity will no longer be proportional to the probe concentration because of fluorescence quenching and fluorescence energy transfer that will occur. This can dramatically affect measured value of *D*.

Second, labeling should be performed in the way one can be assured that the probe is located in the membrane under investigation. This condition is valid for any kind of probe techniques including FRAP and ESR experiments.

A large variety of lipids has been studied by FRAP using different probes. These studies include natural lipids (e.g. egg-PC [19, 20]) as well as artificial membranes (e.g. DMPC [21, 22]). Values of *D* ranged from 10^{-8} cm^2s^{-1} to $8 \cdot 10^{-8}$ cm^2s^{-1} for the systems in the liquid phase. For the gel phase, values of *D* fall between 10^{-11} cm^2s^{-1} (e.g. DMPC [23]) and $5 \cdot 10^{-10}$ cm^2s^{-1} (e.g. DPPC [19]).

2.2 SHORT-RANGE DIFFUSION MEASUREMENTS

2.2.1 Fluorescence quenching

Fluorescence quenching is a phenomenon which decreases the intensity of fluorescence. Several mechanisms can contribute to quenching, but the most important for us is collisional or dynamic quenching.

Bimolecular reaction can illustrate the quenching process

$$F^* + Q \rightarrow F + Q + h\nu \tag{2}$$

where F^* is the excited fluorophore and Q is quencher [9].

The Stern-Volmer theory can be used to explain the diffusion controlled dynamic quenching in isotropic solutions. In this case, diffusion-controlled reaction means that quenching happens on almost any collisions; hence the rate of quenching is governed by the rate at which molecules encounter each other.

The dependence of the emission intensity, I on quencher concentration [Q] is described by the Stern-Volmer equation:

$$\frac{I_0}{I} = \frac{\tau_0}{\tau} = 1 + k_q \tau_0 [Q] \tag{3}$$

where τ and τ_0, in seconds, are the lifetimes of the fluorophore in the presence and absence of quenchers, respectively, k_q, in 1/mole/s, is the bimolecular rate constant for the quenching process.

The product of $k_q \tau_0$ is called the Stern-Volmer constant.

Fato *et al.* used the fact that Stern-Volmer constant is proportional to the sum of initial diffusion coefficients of the fluorophore and quencher to study lateral diffusion in model membranes [24, 25]. They found that diffusion coefficients of phospholipids were higher than 10^{-6} cm^2s^{-1} at 25 ^{0}C. In order to improve the theory of dynamic fluorescence quenching, Owen [26] developed a modified Stern-Volmer treatment, which has taken into account the difference between two-dimensional environment like a lipid membrane and more familiar three-dimensional case.

Lateral diffusion coefficients in membrane are very often overestimated by an order of magnitude or more when Stern-Volmer theory is applied. In fact, this theory is not very applicable to membranes which have significant nonlinearity related to static quenching [27]. The studies demonstrate that nonlinear dynamic quenching is typical for membranes, and that the linear Stern-Volmer model is not a good approximation. The alternative solution is to use numerical analysis to estimate *D*. Corrected treatment showed the value of *D* equals to $1.3\text{-}3.5 \cdot 10^{-7}$ cm^2s^{-1} for soya bean phosphatidylcholine liposomes [27].

Caruso *et al.* [28, 29] studied dynamic quenching of fluorescent probes by time resolved fluorescence experiments. Diffusion coefficients were determined using modified Stern-Volmer model. In this case, the fluorescence quenching of the pyrene derivatives in a monolayer system gave value of *D* in the order of 10^{-7} cm^2s^{-1}.

2.2.2 Fluorescence energy transfer

Fluorescence energy transfer is a mechanism of the excited state interaction where emission of one fluorophore is coupled to the excitation of another. This radiationless process can occur only if energy level difference of neighboring fluorophores corresponds to the quantum of excitation energy. The rate of excitation energy transfer depends on the distance between donor and acceptor molecules.

The quantitative parameter characterizing the efficiency of energy transfer is called the transfer efficiency *E*. Essentially, this is a partial decrease in donor fluorescence because of energy transfer:

$$E = k_T /(k_T + k_0) = 1 - \tau / \tau_0 = 1 - Q / Q_0 \qquad (4)$$

where k_T is the rate constant for dipole-dipole energy transfer between a donor and an acceptor, k_0 is the rate constant for emission of the donor without energy transfer, $\tau = (k_0 + k_T)^{-1}$, $\tau_0 = 1/k_0$ and Q and Q_0 are the quantum yields (donor) with and without energy transfer [30].

Stryer *et al.* reviewed how diffusion affects fluorescence energy transfer efficiency [30]. In general, collisions between donor and acceptor molecules do not contribute to this process. However, energy transfer might be enhanced by diffusion if the distance traversed during the excited state lifetime of the donor is comparable to or larger than the mean distance between donors and acceptors [30]. The relevant parameter in determining the effect of diffusion on transfer is $D\tau_0/r^2$, where D is the sum of the diffusion coefficients of the donor and acceptor, τ_0 is the lifetime of the donor in the absence of transfer, and r is the average distance between donors and acceptors. Three cases can be characterized, but only under the *rapid-diffusion limit*, related to $D\tau_0/r^2 >> 1$ fluorescence energy transfer can be used to measure translational motions. This limit can be achieved by utilizing terbium or other luminescent lanthanides since these donor molecules have lifetimes in the order of milliseconds. Thomas *et al* determined proportionality between the transfer efficiency and the diffusion coefficient in three dimensions [31]. According to this calculated dependence translational motions with D ranging from 10^{-6} to 10^{-10} cm^2s^{-1} can be measured using these donor molecules [30].

2.2.3 NMR spectroscopy

Pulsed field gradient spin-echo method [32-34] has been widely used to study lateral diffusion of the lipid molecules.

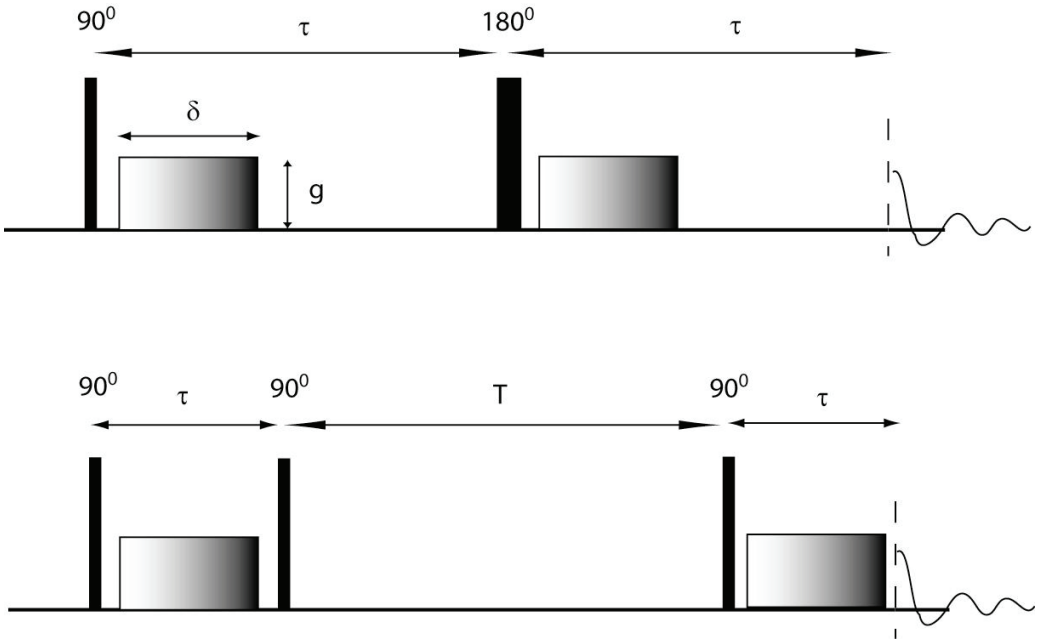

Figure 3 The pulse sequences used in NMR diffusion experiments. Top: spin-echo experiment. Bottom: stimulated spin-echo experiment. The gradient rectangles represent the magnetic field gradient pulses. The r.f. pulses are shown as black rectangles.

There are two main spin-echo experiments for measuring diffusion (see Figure 3). In the spin-echo experiment [35] echo signal is produced at the time 2τ by a pulse sequence ($\pi/2$ - τ -π) illustrated in Figure 3, top. Essentially, the first pulse creates transverse magnetization, after that, nuclear spins with different precessional rates start to dephase in the xy plane. At a time τ, all precessional components are inverted by applying 180^0 radiofrequency pulse. Then, the nuclear spins begin to rephase and finally they meet in order to form an echo. Large field gradient pulses

of strength g and duration δ are imposed on the sample during the dephasing and rephasing periods (just before and just after the π-pulse). The magnitude of the echo, measured at the different separation times τ (see Figure 3) depends on the diffusion of nuclear spins (molecules) through the magnetic field gradients. The diffusion coefficient, D can be obtained in the straightforward way. Magnetic field gradients force the different nuclear spins to precess at different Larmor frequencies, enhancing the dephasing process. If the spins diffuse during the experiment, their precessional rates will change as well, and the precessional components in the xy plane will not refocus completely. This results in the decreasing magnitude of the echo.

In systems with large static dipolar interactions and where transverse relaxation time T_2 is short, sample has to be oriented at the so-called "magic" angle of 54.7^0 with respect to magnetic field B_0. All static interactions have the same term $\frac{1}{2}(3\cos^2\theta - 1)$, where θ is the angle between the bilayer normal and the static magnetic field B_0. When θ=54.7^0, the scaling term $\frac{1}{2}(3\cos^2\theta - 1)$ becomes 0 and the static interactions vanish [36].

The diffusion time can be elongated by using the stimulated spin-echo experiment [37] (Figure 3, bottom). In this case, the diffusion time can be in the order of the longitudinal relaxation time, T_1 which usually much longer then T_2. Thus, this sequence can be used in systems where fast transverse relaxation forbids long τ values. Here, for a time T between dephasing and rephrasing pulses, the net magnetization of a sample can be stored along the z-axis.

Commonly, only δ or g, as well as τ are varied in a diffusion experiment, keeping other parameters constant. The diffusion coefficient D can be obtained from non-linear fit of the data [36].

Because of the improved pulse sequences and advanced hardware, now is possible to use macroscopically non-oriented lipid systems [38, 39]. Cullis *at al.* [40] measured the diffusion of lipids by studing the ^{31}P NMR linewidths as a function of solution viscosity in sonicated vesicles. The authors varied the solution viscosity over a large range in order to reach a condition when the contribution from lateral diffusion was approximately equal to the contribution from vesicle tumbling. By doing this, Cullis employed a simple equation for the lineshape analysis and determined the following values of D: $2 \cdot 10^{-8}$ cm^2s^{-1} and 10^{-9} cm^2s^{-1} in the liquid crystalline and gel phase, respectively. For phospholipid bilayer vesicles these NMR approaches give D values in the order of 10^{-8} cm^2s^{-1}. These values are relatively close to those measured by the FRAP technique.

Note that the time-scale of the experiments can be crucial for the discussion about diffusion coefficient values determined by the different methods. The time-scale of the NMR diffusion technique is in the order of milliseconds. That means for a lipid in liquid state D is obtained over a quite large distance $d \sim 100$ nm. Thus, gradient NMR spectroscopy approach is in between the collisional methods ($d \sim 1$ nm) and the FRAP techniques ($d \sim 10$ μm) [1].

In fact, only artificial membranes have been studied by these approaches.

2.2.4 ESR Spectroscopy

ESR is the name given to the process of resonant absorption or emission of microwave radiation by paramagnetic ions or molecules with at least one unpaired electron spin, and in the presence of a static magnetic field. Special features of ESR that provide unique power for biological studies are that (a) the method detects only unpaired electrons; (b) ESR can see unpaired electrons in any phase and over a wide range of temperatures.

Commonly, membranes do not have intrinsic paramagnetism and thus do not give rise to an ESR spectrum. By inserting a "spin label" (stable free radical) one can employ ESR spectroscopy to shed light on particular environment within the membrane. The typical spin label that is used is the nitroxide free radical.

Formally, an ESR spectrum can be described by the spin Hamiltonian. The interactions of electron and nuclear spins with external magnetic field, B_0 and with each other can be understood using the Hamiltonian

$$\hat{H} = \beta_e \overrightarrow{B_0} \cdot \overline{\overline{g}} \cdot \hat{S} + \hat{I} \cdot \overline{\overline{A}} \cdot \hat{S} \tag{5}$$

where β_e is Bohr magnetron, $\vec{B}_0$ is the external magnetic field, $\overline{\overline{g}}$ is g-tensor, $\hat{S}$ and $\hat{I}$ denotes electron and nuclear spin angular momentum operator, respectively, and $\overline{\overline{A}}$ is an anisotropic hyperfine tensor. The first term is the *electron Zeeman term*, which describes the interaction of the electron spin with the external magnetic field. The second term represents the *hyperfine interaction*, which is due to the interaction of the electron spin with magnetic moment of ^{14}N nuclear spin. The *g* and hyperfine terms are orientation dependent. The hyperfine interaction is maximum along the *p* orbital of the nitrogen (A_{zz}~32 G, see Figure 4) and minimum in the plane perpendicular to the *p* orbital ($A_{xx}=A_{yy}$~6 G). Furthermore g-value is anisotropic as well: the principal values of g-tensor are g_{xx}~2.0090 (maximum, along the N-O bond), g_{zz}~2.0025 (minimum, along the *p* orbital) and g_{yy}~2.0060 (intermediate, along the y axis in the molecular frame).

If the molecule is rapidly tumbling (i.e., motional narrowing regime) anisotropic terms are averaged out to first order and the Hamiltonian is reduced to

$$\hat{H} = g\beta_e B_z \hat{S}_z + A\hat{I}_z \hat{S}_z \qquad (6)$$

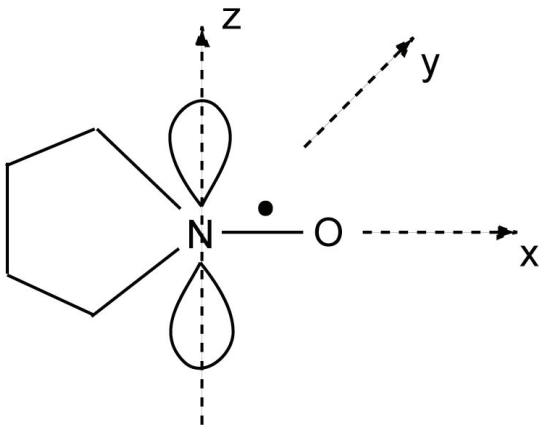

Figure 4 Molecular axes of the nitroxide

Here g and A is reduced to the isotropic g and hyperfine components due to fast, isotropic motion which completely eliminates the $\overline{\overline{g}}$ and $\overline{\overline{A}}$ anisotropy. The energy level diagram of the nitroxide that is obtained from equation (6) is shown in Figure 5. In the absence of external magnetic field electron energy levels are degenerate. When static magnetic field is applied, the degeneracy is lifted. This happens because electron spins with parallel and antiparallel orientation have different energy in the presence of magnetic field (*Zeeman interaction*, frequency of transition is on the order of 9 GHz for B_0=3400 Gauss). Additionally, the electron spin energy levels are split due to the *hyperfine interaction* (these transitions are on the order of several MHz). The electron spin

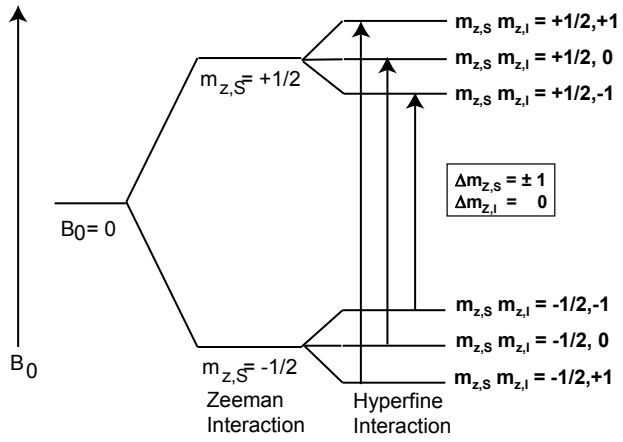

Figure 5 Energy diagram showing the three transitions of nitroxide**.** Symbols $m_{z,S}$ and $m_{z,I}$ represent electron and nuclear angular momentum quantum numbers, respectively.

levels split into ($2I + 1$) sublevels by every nucleus of spin I. Since ^{14}N of the nitroxide has I=1 the energy level diagram reveals the three allowed transitions, resulting in the distinct three-line nitroxide-specific spectrum, shown in Figure 6, top.

The width of the spectral line is due to *homogeneous broadening* and *inhomogeneous broadening*. If all spins experience the same magnetic field and have the same spin-hamiltonian parameters, then the spin system ("spin packet") gives rise to a so-called the homogeneous line broadening [41]. These are due to modulation of the electron-nuclear dipolar (END) interaction, and the electron-electron dipolar (EED) interaction by molecular motion. They discussed in detail later. Essentially, all spins have the same linewidth resulting in the characteristic Lorentzian shape.

Now, one can consider that every spin experiences a slightly different local field. In this case, the observed spectrum line is a superposition of a large number of spin packets, each shifted from the others. This lineshape is essentially an envelope of contributions from all spins and inhomogeneously broadened. The lineshape will be characterized by Gaussian. The composition of lipid vesicles is a good example of the system giving natural inhomogeneous broadening. In this case, the system is macroscopically disordered, because each lipid bilayer has a different orientation with respect to B_0. Hence the contribution from each bilayer has slightly different values of A and g tensors, leading to a broadening of the hyperfine lines [42]. At the same time, since the bilayer is a sheet-like organized structure there is a significant microscopic ordering. These biological systems might be referred as MOMD (i.e. microscopically ordered but macroscopically disordered) case [43]. In the case of the lipid systems, all possible orientations of the spin-labeled moieties give rise to a broad spectrum (see below) with significant inhomogeneous broadening superimposed on the homogeneous linewidth. This MOMD effect

(inhomogeneous broadening) conceals the homogeneous lineshape leading to the loss of the spectral resolution.

From equation 6, the splitting of the hyperfine structure changes with the orientation of the static magnetic field with respect to the reference frame of the nitroxide. This spectral anisotropy makes ESR very sensitive to the molecular motions, especially rotational and translational diffusion [44].

The two extreme cases of how rotational reorientational motion gives rise to a different ESR lineshapes can be considered. For a sample where the molecule tumbling randomly in a non-viscous solution (motionally narrowed limit, rotational correlation time $\tau_r<10^{-10}$ s), one obtains an isotropic spectrum with three narrow lines which does not depend on the magnetic field orientation (Figure 6, top). The opposite extreme to the isotropic spectrum is a rigid limit spectrum. In this case, the molecule rotates with a rate that does not exceed the linewidth ($\tau_r>10^{-6}$ s), the spectrum appears static (Figure 6, bottom). It consists of a superposition of spectra of every possible orientation of molecular axes with respect to B_0, i.e. to a *powder spectrum*.

For the intermediate case, the spectrum is broadened and one can determine τ_r by comparing experimental spectrum with linewidth simulations. For instance, there might be rotational anisotropy i.e. because of its different shape, the molecule can rotate with various rates about different axes. Rod-shaped molecule has greater probability to rotate about its long axis. This results in a different lineshape than the rotation of roughly sphere-shaped molecule. In the same way, attachment of a side-chain to a macromolecule gives rise to the lineshape of the side-chain moving in the potential of the slowly tumbling macromolecule. Analysis of these lineshapes allows one to determine which processes influence the dynamics of the system under investigation.

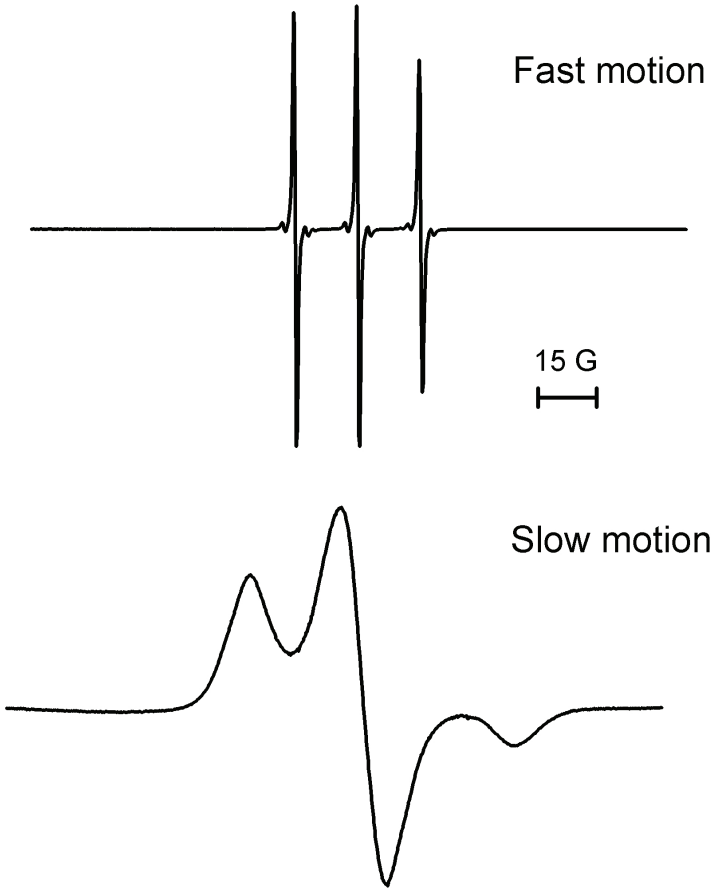

Figure 6 Continuous wave nitroxide spectrum under different conditions. Top: motionally narrowed limit (i.e fast motion). Bottom: rigid limit (i.e. slow motion). The scale is the same for both graphs

To analyze spectral lineshape the second order effects, which creates homogeneous broadening, have to be accounted for. These include broadening from intramolecular electron-nuclear dipolar (END) interaction, Heisenberg spin exchange and the magnetic dipole-dipole interactions. END mechanism dominates at low temperatures and concentrations. In this case, the significant contributions come from anisotropic interactions in the nitroxides themselves. Molecular tumbling modulates the END hyperfine interaction contributing to the nuclear spin flips. The magnetic field due to the presence of the unpaired electron spin in the rapidly

reorienting nitroxide is modulated by rotational diffusion leading to an important nuclear relaxation mechanism. When concentration of spin label is relatively high there is the line broadening caused by the presence of intermolecular spin-spin interactions. Two mechanisms contribute to this: the Heisenberg Exchange (HE) interaction and the dipole-dipole interaction. HE is essentially a contact interaction between nitroxide radicals. When radicals collide the wave functions of the two unpaired electrons strongly overlap for a short time [45]. The fundamental parameter of this process is the spin-label exchange frequency ω_{ex}, which is directly related to the collision frequency ν_{coll}. Hence, HE can be used to measure the rate of bimolecular collisions and therefore enables one to study translational diffusion.

The Heisenberg spin exchange can be described by spin Hamiltonian [9]

$$H_{ex} = -2J \cdot \vec{S}_1 \cdot \vec{S}_2 \tag{7}$$

where J is so-called the exchange integral (the magnitude of exchange interaction) and the index 1 and 2 represent the electron spins of the first and second nitroxides, respectively. The magnitude of the spin-spin exchange interaction J in this case can be expressed in terms of an exchange frequency ω_{ex}

$$J = h\omega_{ex} \tag{8}$$

where h is Plank's constant.

Two cases can be considered [9]: The so-called weak exchange and strong exchange. In the first case, (weak exchange $\omega_{ex} << a_N$, where a_N is the hyperfine interaction) there is a

noticeable line broadening, but positions of the lines stay the same. In the second case, (strong exchange, $\omega_{ex}>>a_N$) three-line hyperfine spectrum becomes a single Lorentzian line spectrum due to the exchange narrowing.

Magnetic dipole-dipole interaction depends on the distance between spin labels and can be used to measure intermolecular separations. This interaction is inversely proportional to the spin-label separation cubed and is also orientation dependent. The dipolar Hamiltonian for the electron dipolar interaction is

$$\hat{H}_{dd} = \left(\frac{g^2 \beta_e^2}{r^3} \right) \left(3\cos^2\theta - 1\right)\left(\hat{S}_1 \hat{S}_2 - 3\hat{S}_{1Z}\hat{S}_{2Z}\right) \tag{9}$$

where r is the distance between two electrons and θ is the angle between the interspin vector r and the direction of the external magnetic field.

Furthermore, magnetic dipole-dipole interaction can be completely averaged out to first order by isotropic motion, i.e.

$$< 3\cos^2\theta - 1 >= 0 \tag{10}$$

In order to get significant broadening due to spin-spin interaction, high spin-label concentrations (> 2 mol %) are required. At low concentrations, the HE and dipolar contributions to the interaction broadening can be separated by the temperature dependence (via their inverse dependence on the diffusion coefficient) and the linewidth simulation studies [46].

In the context of studying translational motion of lipids in natural and artificial membranes, Trauble and Sackman [47] performed a simulation of ESR spectra. This theoretical analysis of the spectral linewidth yields HE frequencies ω_{ex}, which in turn is very easily related to the diffusion coefficient D. Essentially, these authors regard the process as a homogeneous, two-dimensional diffusion. In this case, the collision frequency

$$\nu_{coll} = 3 \cdot \omega_{ex} = \frac{8 d_c}{F \cdot \lambda} \cdot D \cdot c \tag{11}$$

where d_c is the effective interaction distance between nitroxides, F is the area per lipid molecule, λ is the length of one jump, c is the mole fraction of the spin label.

For the androstane derivative spin-label in fluid bilayers of dipalmitoylphosphatidylcholine (DPPC), Trauble and Sackman assumed: F =58 Å^2, λ =8 Å, d_c = 20 Å, and D was estimated to be ~ 10^{-8} cm^{2}s^{-1}. The value of F was obtained from X-ray studies, λ was determined by the lattice constant, d_c was predicted by theoretical studies [48].

Devaux and McConnell [49] used rather different approach to evaluate D. Basically, changes in the observed ESR spectra of highly concentrated region of a spin-labeled phosphatidylcholine (PC) incorporated into oriented bilayers of PC were monitored over time. This time dependence is caused by the lateral diffusion of the oriented labeled molecules moving in the plane of the corresponding monolayers. The estimated value of D was ~ $1.8 \cdot 10^{-8}$ cm^{2}s^{-1}.

An alternative method was introduced by Popp and Hyde [50]. Continuous wave electron-electron double resonance spectroscopy (ELDOR) approach was used to measure the bimolecular collision frequency between steric acid spin-labels in

dimyristoylphosphatidylcholine (DMPC) bilayers. They studied the rate of saturation transfer between the low-field (M_I=+1) and center (M_I=0) lines of the nitroxide spectrum. There are three saturation-transfer mechanisms which can be probed by ELDOR technique: HE, nitrogen nuclear relaxation and slow rotational diffusion [46]. The last two are intramolecular while the first is intermolecular and proportional to the concentration of the label. By changing the spin-label concentration they managed to distinguish the exchange and nuclear relaxation contributions to the ELDOR process. This method provided values of *D* which are in a good agreement with the values obtained by the other techniques, i.e., on the order of $5 \cdot 10^{-8}$ $cm^2 s^{-1}$.

The contribution of the electron-nuclear dipole (END) induced nuclear relaxation can dominate, especially under low temperatures (< 27 ^{0}C for DMPC [50]). This can make the process of obtaining ω_{ex} not feasible. Difficulty due to the presence of END nuclear relaxation can be resolved by using ^{14}N:^{15}N spin-label pairs for ELDOR studies [51]. The idea of this experiment is to excite one spin system and observe the saturation transfer to the other spin system. Although there is a presence of intramolecular END mechanism for each spin system, there is no coupling between ^{14}N and ^{15}N systems. Only intramolecular mechanisms (HE and dipolar interaction) contribute to the saturation transfer, hence one can measure HE rates and the bimolecular collision frequencies. This approach provided *D* values of $4.5 \cdot 10^{-8}$ $cm^2 s^{-1}$, $5.7 \cdot 10^{-8}$ $cm^2 s^{-1}$ and $8.1 \cdot 10^{-8}$ $cm^2 s^{-1}$ for DMPC at the corresponding temperatures 27, 37 and 47^{0}C.

All ELDOR studies mentioned above have been done using conventional continuous wave (CW) techniques. At the same time, HE rates ω_{ex} can be measured with the short-pulse saturation recovery ESR technique [52].

Conventional CW methods have some limitations, for instance relatively low sensitivity. Additionally, inhomogeneous broadening dominates the CW-ESR lineshape. One source of this

inhomogeneity is the so-called MOMD effect, which is particularly relevant to lipids (see above). It is difficult to extract ω_{ex}, since Heisenberg spin exchange relaxation process is weak, and the dominating inhomogeneous broadening cannot be predicted by any equations. In order to remove these limitations, Fourier transform ESR (FT-ESR) spectroscopy has been developed recently [7, 44]. The main merit of this technique is that one can distinguish between different relaxation processes using two orthogonal frequency dimensions as well as cross-relaxation phenomenon. Thus, FT-ESR provides not only increased sensitivity but also principal ability to separate different contributions to the linewidth, a feature that CW-ESR spectroscopy lacks. In the next chapter, we will present discussion about FT-ESR spectroscopy and how it can be applied to study translational diffusion in lipids.

3.0 TWO-DIMENSIONAL FOURIER TRANSFORM ESR

Two-dimensional FT-ESR spectroscopy is an attractive technique to study lateral motion in lipids. As mentioned before, the main disadvantage of CW-ESR is a lack of spectral resolution due to the dominating inhomogeneous broadening. In this case, HE rates are measured *indirectly*. Despite advanced experimental setup that is required for FT-ESR approach, pulse ESR spectroscopy provides *direct* estimation of HE rates and requires a simple analysis scheme (see below).

In the past, only Millhauser *et al* used FT-ESR to study diffusion of spin-labeled peptides [53]. To our knowledge there have been no attempts to evaluate lateral diffusion of lipids using this approach. In order to demonstrate the feasibility of 2D FT-ESR technique to diffusion studies, D of the small spherical probe molecule (perdeuterated tempone, radius $r \sim 3.2$ Å) in the lipid phase has been evaluated (see Section 3.4). In the future, spin label that is rigidly attached to the phospholipid molecule ("doxyl" spin-label [9]) or spin-labeled cholesterol molecule [9] can be used to mimic the motion of the lipids and provide value of D for a given lipid system.

3.1 BASIC CONCEPTS OF FOURIER TRANSFORM ESR

Most of the NMR spectroscopy today and a significant part of ESR spectroscopy rely on pulse irradiation rather then conventional continuous irradiation. NMR spectroscopy based on Fourier Transform has become a standard because of increased sensitivity in comparison with CW techniques. Another reason for wide use of FT-NMR is the development of two-dimensional spectroscopy, which allows structure determination of complex molecules.

In CW spectroscopy, one has to obtain spectrum by sweeping the magnetic field (most common) or microwave frequency. On the other hand, we can measure the overall spectrum by applying short, powerful pulse on the sample. This pulse excites all possible spin transitions simultaneously. In this case, response of the sample contains harmonic oscillation terms reflecting all transition frequencies. This time-decaying signal is termed free induction decay (FID). After collecting the FID signal it is necessary to perform a Fourier transform of the data in order to compute the frequency spectrum (see Figure 7).

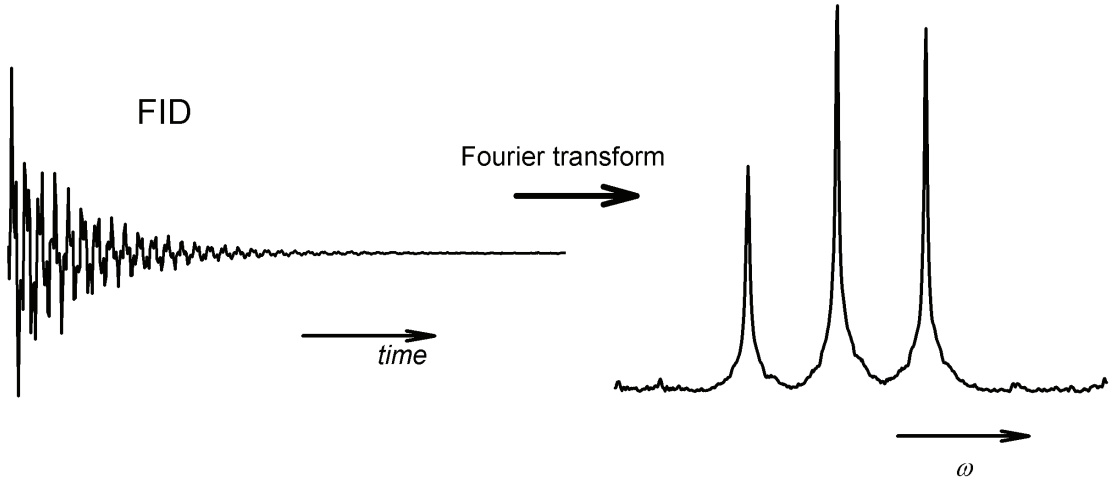

Figure 7 Time domain FID signal and corresponding frequency domain spectrum (after Fourier Transform)

Pulse FT-ESR spectroscopy can be employed in many different ways providing supplementary information on the system of interest. For example information about relaxation times, diffusion constants, distance between spins *et cetera* can be obtained using variants of FT-ESR method.

In order to get the maximum detectable signal, one should apply a pulse of duration t_p to rotate net magnetization in the xy plane ($\pi/2$ pulse). The required power and a pulse length can be estimated by a formula for a flip angle β (rotation angle of the magnetization vector)

$$\beta = \gamma_E B_1 t_p = \frac{\pi}{2} \tag{12}$$

where γ_E is the electron gyromagnetic ratio, B_1 is the strength of applied oscillating magnetic field.

A pulse with $\beta=180^0=\pi$ is sometimes called an inversion pulse because it inverts the magnetization vector. Pulses with $\beta=90^0=\pi/2$ and $\beta=180^0=\pi$ are most common in pulse FT-ESR spectroscopy.

Due to technical limitations, the FID signal cannot be detected immediatly after the pulse, because the energy of the high power microwave pulse (~ 1 kW) cannot dissipate immediately. The FID signal will be perturbed and superimposed by the ring-down from the pulse during the time shorter than the spectrometer dead-time, t_d. In membrane studies, the spin labels have relatively low mobility, which results in the slow-motional broadening [54]. This gives rise to the large inhomogeneous broadening, or, in other words, very fast decaying FID signal. Due to the dead-time effect, there will be a loss of an important part of the signal that leads to the loss of the sensitivity. There was a significant progress in reducing dead-time of commercially available spectrometers [55]. For example a reduction of t_d to ~ 30 ns results in improving the signal-to-noise ratio of detectable signal by a factor of 10 for a sample with short transverse relaxation time T_2. This approach makes FT-ESR applicable to studies of wide range of samples.

3.2 TWO-DIMENSIONAL ELECTRON-ELECTRON DOUBLE RESONANCE

Dynamic processes like rotational and translational diffusion can be investigated by analysis of the lineshapes of CW spectra, but it might be difficult to understand which model is valid for the studied process. FT-ESR can provide more information about the magnetization transfer when system undergoes such processes by following the correlations of ESR spectra at various times. Heisenberg exchange, ^{14}N nuclear spin relaxation, dipolar magnetic interactions are usually the processes that contribute to the correlation of ESR transitions. Fast relaxation processes on the order of longitudinal relaxation time T_1 can be studied by 2D-ELDOR experiment [45]. The 2D-ELDOR pulse sequence is presented in the Figure 8 [8].

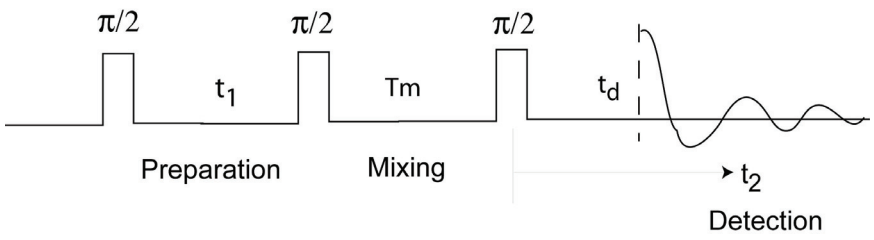

Figure 8 Pulse sequence for 2D-ELDOR experiment

The preparation period consists of a π/2 pulse to create the initial transverse magnetization that evolves for a time t_1. During the evolution period, magnetization components start to dephase in the xy plane. The second π/2 pulse marks the beginning of the mixing period, wherein the longitudinal magnetization components associated with each hyperfine line can be exchanged (magnetization stored at –z direction, to minimize the contribution from fast transverse relaxation T_2), hence giving rise to mixing components carrying different

precessional-frequency information. Then, after rotating this magnetization back into the xy plane by the third $\pi/2$ pulse, components initially precessing with angular frequency $\omega_1=\omega_a$ will precess with new frequency $\omega_2=\omega_b$. The pulse sequence is repeated for a series of evenly spaced values of t_1. For every t_1, the FID is accumulated during a period t_2. Additionally, the pulse sequence is repeated for several different values of the mixing time T_m.

There is a notation of all possible peaks that can be formed in 2D-ELDOR experiment. First of all, the peaks running along diagonal are called "auto-peaks" (Figure 9). These peaks are representing normal ESR spectrum (three ^{14}N hyperfine lines which can be found in the conventional CW spectra). However, there is another principal type of possible peaks in the 2D-ELDOR plot: off-diagonal peaks are termed "cross-peaks" and are formed by connecting different auto-peaks (Figure 9, bottom, cross-peaks are denoted by the red and blue circles). Cross-peaks that are formed by connecting two adjacent auto-peaks are called the first-order cross-peaks (Figure 9, red circles). There are four possible first-order cross peaks located on the 2D plot. Additionally, cross-peaks that are formed by connecting outer auto-peaks are termed the second order cross-peaks (Figure 9, blue circles). There are two possible second order cross-peaks. Finally, there might be nine auto and cross-peaks total on the 2D-ELDOR plot.

There are two mechanisms of formation of the cross-peaks: due to rotational reorientational motion (W_n) and due to Heisenberg spin exchange (ω_{ex}). The essential point is that these different relaxation mechanisms contribute intensity to the different type of cross-peaks. Motionally induced ^{14}N nuclear relaxation (W_n mechanism) obeys selection rule $\Delta M_I=\pm1$, hence only first-order cross peaks are present when this mechanism dominates. At the same time, Heisenberg spin exchange does not have nuclear spin selection rules. In the case of the presence of HE there are comparable first and second-order cross peaks which can be found on the 2D

plot. However, the presence of second order cross-peaks does not always mean the presence of HE. The rotational reorientational motion mechanism can contribute intensity to the formation of these peaks by two consecutive single quantum transitions. This occurs only when the T_m is long enough.

It is clear that visual inequities of the 2D-ELDOR plot can report about different relaxation mechanisms. The presence of only first order cross-peaks provides information that the system does not have significant HE contribution, and W_n mechanism dominates. The contrary case is possible when there is the presence of both first and second-order cross-peaks (Figure 9). In this case, HE mechanism which equally contributes intensity to all cross-peaks has considerable effect on the system.

In a series of experiments the rate of formation of cross-peaks with increasing mixing time T_m is monitored (see Figure 10). Performing 2D-ELDOR on the samples with different concentrations of spin-label at various temperatures can help one to clearly distinguish between these two mechanisms.

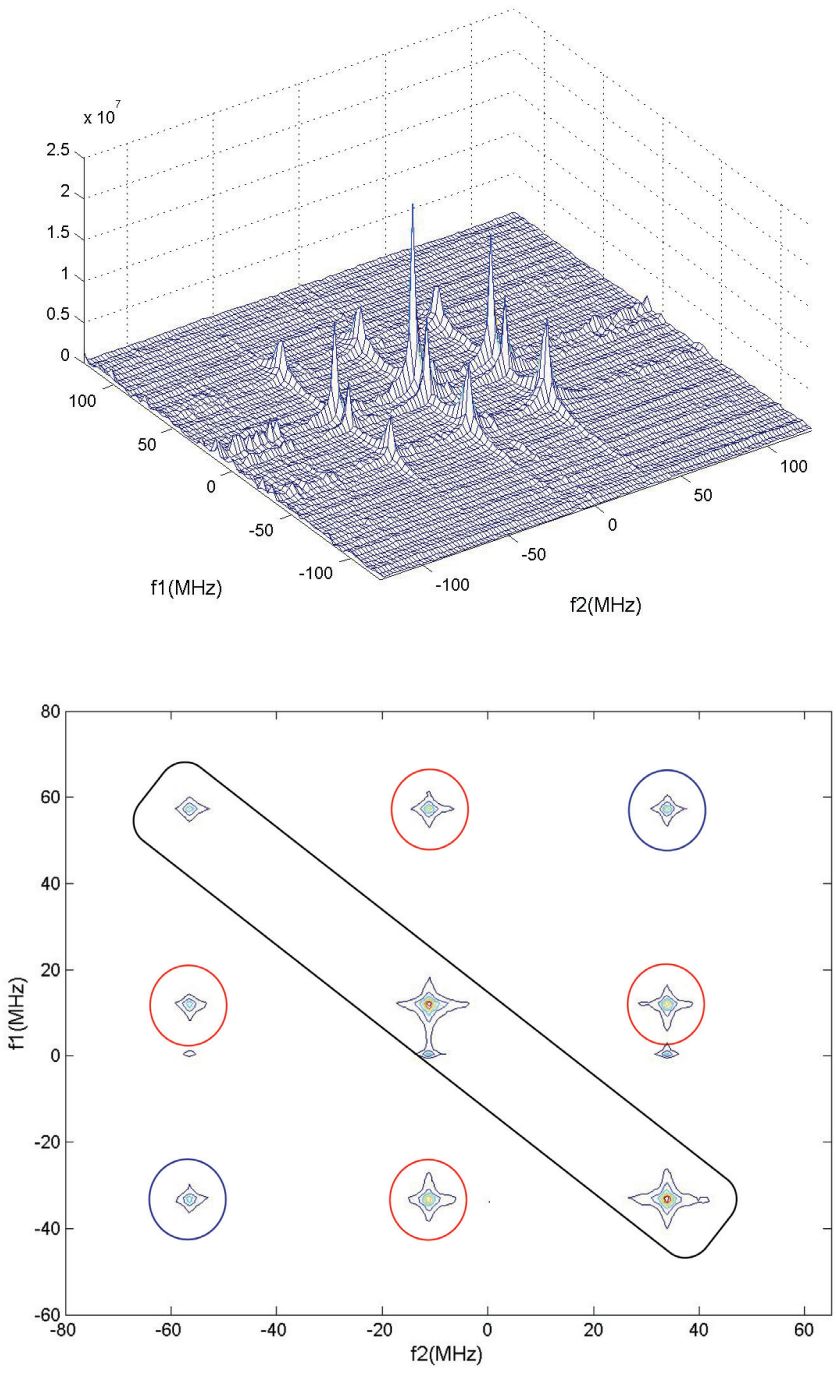

Figure 9 2D-ELDOR absolute-value surface plot (top) and contour plot (bottom) of DphPC lipids and perdeuterated Tempone (4 mol %) at T_m = 1000 ns (room temperature). The diagonal peaks are termed auto-peaks. The off-diagonal cross-peaks (CP) are denoted by red circles (first-order CP) and blue circles (second-order CP)

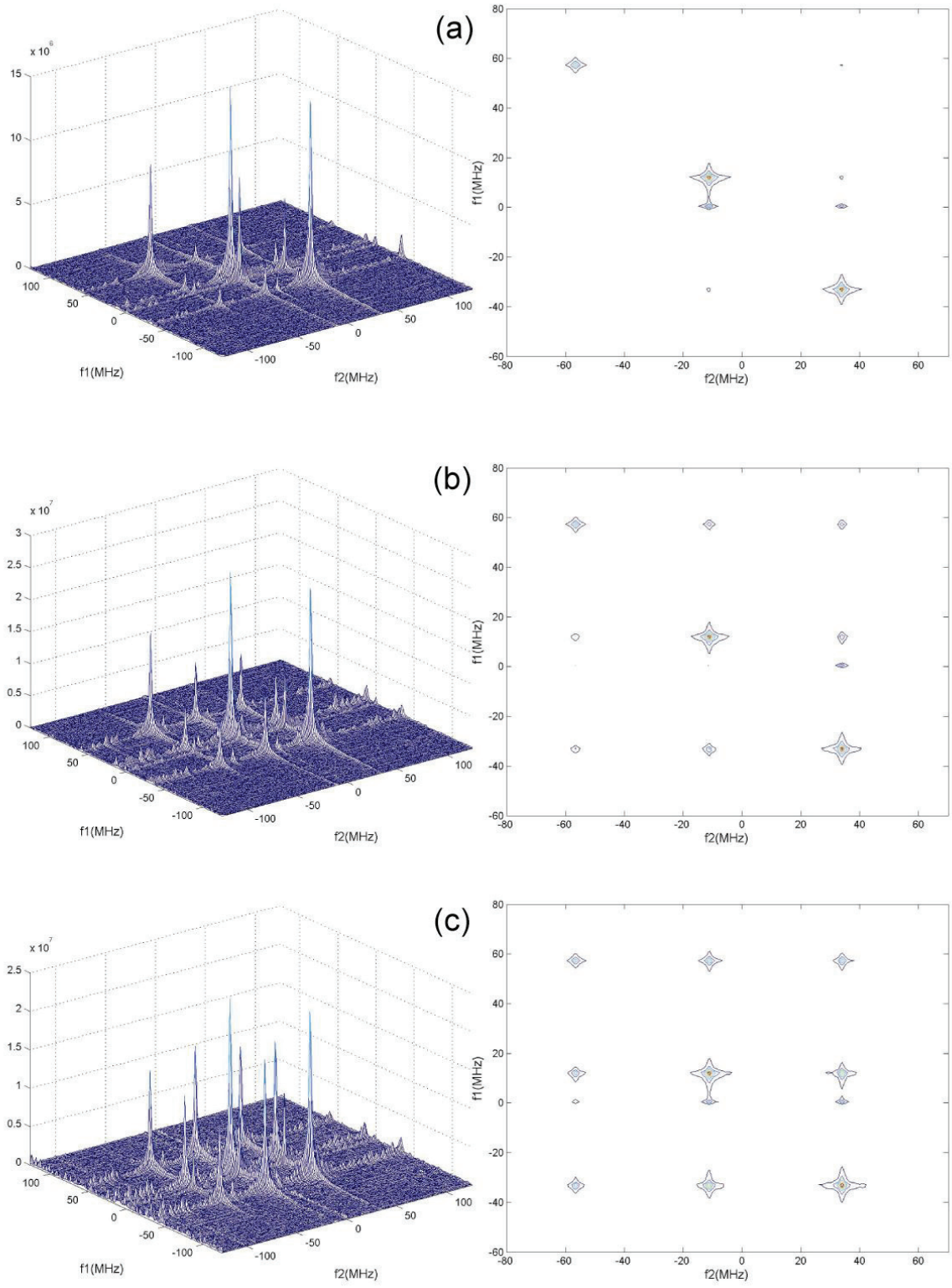

Figure 10 Series of 2D-ELDOR spectra of DphPC lipids and Perdeuterated Tempone (4 mol %) at T = 292 K: (a) T_m=200 ns, (b) T_m=500 ns and (c) T_m=1000 ns

3.3 OBTAINING ω_{ex} AND W_n FROM 2D-ELDOR SPECTRA

In order to extract relaxation rates from the 2D-ELDOR spectra one should consider two procedures. First procedure requires collection of few 2D-ELDOR spectra at different values of the mixing time T_m (usually T_m varies from very small value, i.e. tens of nanoseconds up to few microseconds). The time evolution of every spectral line can be directly monitored [7]. Next step is the simultaneous fitting of the data using the set of stochastic Liouville equations [46] in order to determine W_n and ω_{ex}. This global fitting approach is applicable to fast motion of the spin label as well as slow motion.

Another approach requires careful examination of every 2D spectrum and comparison of the volumes of the auto and cross peaks. As a matter of fact, this approach results in the simple analytical expressions for ω_{ex} and W_n. However, this technique is valid only when the system is in the fast motional regime (room temperature, non-viscous solution). We will discuss this approach in more detail now.

In the case when 2D peaks are pure Lorentzian (inhomogeneous broadening is negligible), one can use peak amplitudes for quantitative studies rather than peak volumes.

Gorcester and Freed developed the theory for 2D-ELDOR experiment [7]. In general, in the presence of both W_n and ω_{ex}, it is necessary to solve a full set of linear equations [56]

$$\left(2f_{+1,0} + V_{+1}r_{2_{+1}}\right)c = \left(V_{+1}r_{2_{+1}} - f_{+1,0}\right) \tag{13}$$

$$\left(2f_{-1,0} + V_{-1}r_{2_{-1}}\right)c = \left(V_{-1}r_{2_{-1}} - f_{-1,0}\right) \tag{14}$$

$$\tfrac{3}{2}\left(f_{0,+1}V_{+1}r_{2_{+1}}\right)b + \left(1 + \tfrac{1}{2}f_{0,+1}V_{+1}r_{2_{+1}}\right)c = \left(1 - f_{0,+1}V_{+1}r_{2_{+1}}\right) \tag{15}$$

$$\tfrac{3}{2}\left(f_{0,-1}V_{-1}r_{2_{-1}}\right)b + \left(1 + \tfrac{1}{2}f_{0,-1}V_{-1}r_{2_{-1}}\right)c = \left(1 - f_{0,-1}V_{-1}r_{2_{-1}}\right) \tag{16}$$

$$\tfrac{1}{2}\left(V_{+1}r_{2_{+1}} + f_{+1,-1}V_{-1}r_{2_{-1}}\right)b + \tfrac{1}{6}\left(f_{+1,-1}V_{-1}r_{2_{-1}} - V_{+1}r_{2_{+1}}\right)c = \tfrac{1}{3}\left(V_{+1}r_{2_{+1}} - f_{+1,-1}V_{-1}r_{2_{-1}}\right) \quad (17)$$

$$\tfrac{1}{2}\left(V_{-1}r_{2_{-1}} + f_{-1,+1}V_{+1}r_{2_{+1}}\right)b + \tfrac{1}{6}\left(f_{-1,+1}V_{+1}r_{2_{+1}} - V_{-1}r_{2_{-1}}\right)c = \tfrac{1}{3}\left(V_{-1}r_{2_{-1}} - f_{-1,+1}V_{+1}r_{2_{+1}}\right) \quad (18)$$

where $b = \exp[-(2W_n + \omega_{ex})T_m]$ and $c = \exp[-(6W_n + \omega_{ex})T_m]$.

Let us discuss the notation that we introduced in equations (13)-(18). Parameter f_{mj} represents the volume ratio of the cross peak at position (ω_1, ω_2) = (ω_m, ω_j) to the auto peak at (ω_j, ω_j) or in other words $f_{mj} \equiv Q_{mj} / Q_{jj}$, where Q denotes the volume of a given peak. Figure 11 illustrates the

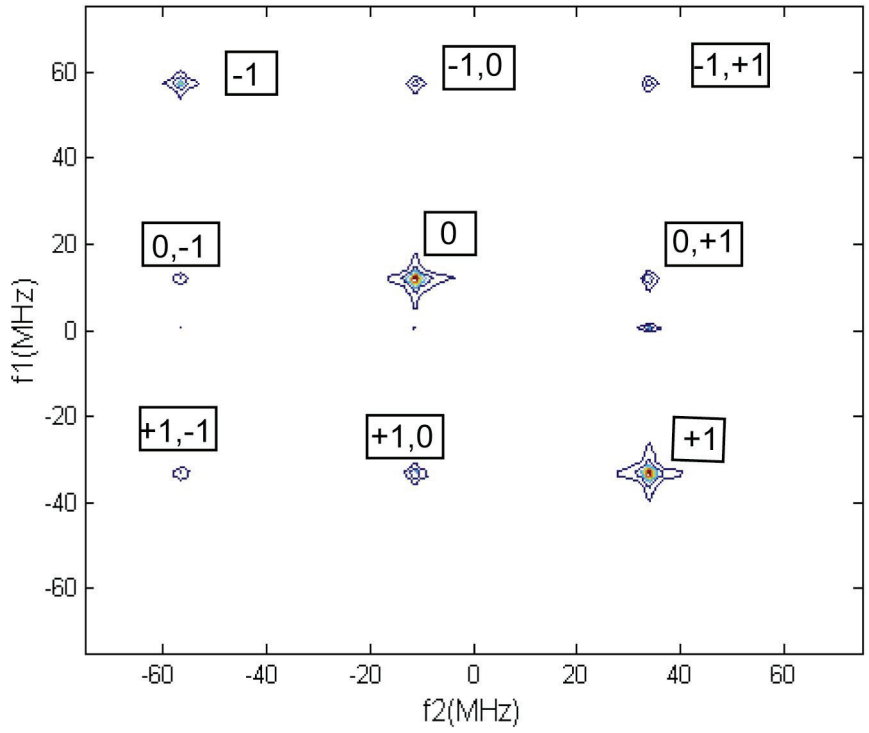

Figure 11 Notation of the 2D-ELDOR auto and cross peaks. Diagonal peaks which represent normal CW-ESR spectrum (symbols -1, 0 and +1 for three hyperfine lines). Off-diagonal cross-peaks are identified by (ω_1, ω_2) = (ω_m, ω_j)

labelling scheme for all possible nitroxide peaks, diagonal auto peaks are denoted by symbols -1, 0 and +1, representing three hyperfine lines. The peak volumes might be estimated by integration of every 2D line. Essentially, one can numerically integrate in the ω_2 domain (calculate the area of a slice) and sum the resulting numbers over the separate values of ω_1 [57].

There are two attenuation factors that need to be considered. Parameter V_j of a given nitroxide line *j* takes into account limited excitation bandwidth (i.e. rotation of a given hyperfine line by less than $\pi/2$ angle). It might be because of the insufficient oscillating magnetic field B_1 at the position of the sample or the limited bandwidth of the resonator due to its finite quality factor Q. The example of the excitation profile is shown on Figure 12.

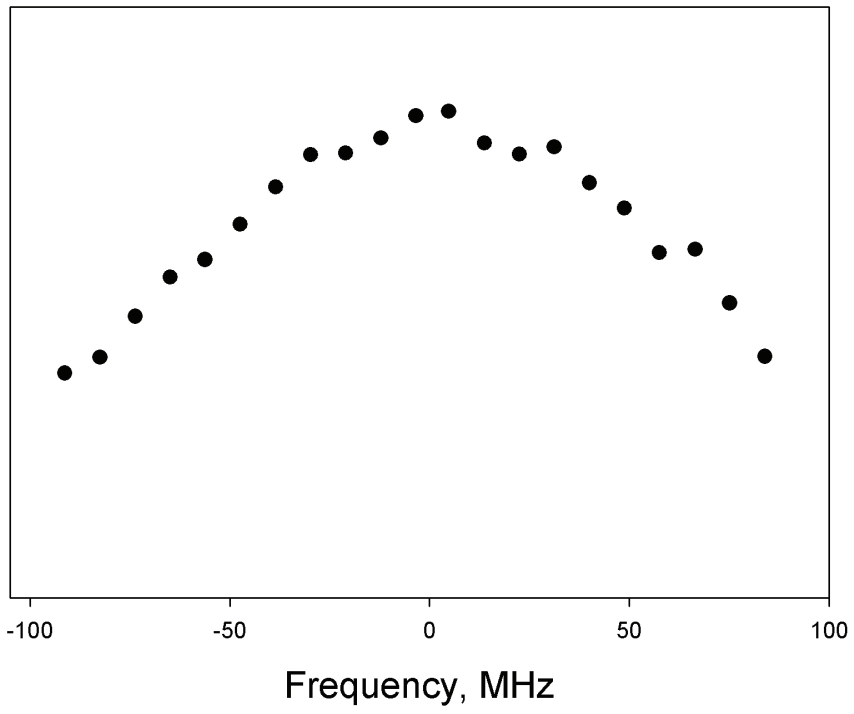

Figure 12 Excitation profile of the pulse FT-ESR spectrometer (T=292 K)

The presence of the dead-time reduces the detectable signal. The parameter r_{2j} of a given hyperfine line j estimates the reduction due to the dead-time effect and can be calculated from equation

$$r_{2_j} = \exp(-\tau_{d_2} / T_{2_j}^*) \tag{19}$$

where τ_{d2} is the dead-time in t_2 dimension, $T_{2_j}^*$ is the inhomogeneous transverse relaxation time of a given nitroxide line and can be estimated from the CW spectra using the peak-to-peak linewidth of the given hyperfine component.

Instead of calculating parameters V_j and r_{2j} separately they can be determined simultaneously as the products $V_j r_{2j}$ in the equations (13)-(18). In this case, the products $V_j r_{2j}$ are obtained by measuring the normalized peak areas using a single pulse FID experiment ("coverage" experiment) [56]. This "coverage" experiment should be performed under the same conditions (e.g. pulse length t_p, resonator quality factor Q, microwave frequency etc.) as the actual 2D-ELDOR experiment.

After solving overdetermined system of six linear equations one can estimate values of W_n and ω_{ex} from the equations [56] for each value of the mixing time T_m

$$2W_n = \frac{1}{2T_m} \ln\left(\frac{b}{c}\right) \tag{20}$$

and

$$\omega_{ex} = \frac{1}{2T_m} (\ln c - 3\ln b) \tag{21}$$

There is a simple case when the overdetermined system of six linear equations reduces to a single equation. This specific case might be considered in the system where HE is the only contribution to the magnetization transfer, namely

$$\omega_{ex} = \frac{1}{T_m} \ln\left(\frac{2 f_{mj} V_j r_{2_j} + V_m r_{2_m}}{V_m r_{2_m} - f_{mj} V_j r_{2_j}} \right) \tag{22}$$

here we used the same notation as we introduced in equations (13)-(18). When $W_n \neq \omega_{ex} \neq 0$ the overdetermined system of six linear equations should be considered.

3.4 EXPERIMENTAL SECTION

3.4.1 Sample preparation

2D-ELDOR experiments have been performed on the sample of diphytanoylphosphatidylcholine (DphPC) that does not have a phase transition in the measured range of -120 ^{0}C to +120 ^{0}C. This phospholipid sample was mixed with a water-soluble spin label 4-Oxo-Tempo-d_{16}, which easily partitions between the aqueous and lipid phase. DphPC was purchased from Avanti Polar Lipids, Inc. Alabaster, AL. 4-Oxo-Tempo-d_{16} spin label was purchased from Aldrich. A measured amount of 35.5 mM 4-Oxo-Tempo-d_{16} in stock solution was added to 41.5 mg of DphPC in excess chloroform to produce 4 mol %. The chloroform was then evaporated under flowing nitrogen and the sample was put under vacuum for 30 minutes to

remove residual solvent. A small amount of aqueous phase was added to form a saturated dispersion. Finally, the sample was sonicated to produce small, single-bilayer vesicles with roughly the same diameter.

3.4.2 ESR spectroscopy

The ESR experiments were performed on Bruker EleXsys E580 CW/FT X-band ESR spectrometer. The spectra were collected with a Bruker ER 4118X-MS3 X-band loop-gap resonator. The length of the π/2 pulse was 6 ns. The number of points in t_1 and t_2 were 512 with a step size of 4 ns. The number of averages was ranged from 500 to 40 K. The dead time t_d in t_2 dimension was around 40 ns. Experiments were performed at four temperatures: 273, 283, 292 and 310 K.

3.4.3 Results

As stated above, the volumes of 2D peaks were estimated by numerical integration in the f_2 domain (calculate the area of a slice) and summing the resulting numbers over the discrete values of f_1. The important step is to define the correct range in f_1 and f_2 dimensions for each peak in order to minimize the possible integration errors. After getting the peak volumes, the coverage reduction factors V_j and r_{2j} should be calculated as described before. It is worth stressing that only attenuation parameters for +1 and -1 hyperfine lines need to be determined (i.e. V_{-1}, V_{+1}, r_{21} and r_{2+2}) because V_0 and r_{20} is conveniently assumed to be equal to unity. Parameters V_{-1} and V_{+1} were estimated from single pulse FID ("coverage") experiment for every temperature. Factors r_{21} and r_{2+2} were calculated using equation (19), where $T_{2_j}^*$ was determined

from CW experiments, as it was explained before. Attenuation parameters for four temperatures presented in Table 1.

Table 1 Coverage attenuation parameters and their products

	V_{-1}	V_{+1}	$r_{2(-1)}$	$r_{2(+1)}$	$V_{-1}*r_{2(-1)}$	$V_{+1}*R_{2(+1)}$
273K	0.795	1	0.907	0.915	0.721	0.915
283K	0.505	0.899	0.913	0.936	0.461	0.841
292K	0.718	0.96	0.906	0.923	0.651	0.886
310K	0.761	0.95	0.902	0.908	0.686	0.863

The peak volume ratios as well as the spectrometer coverage attenuation factors for five and more mixing times were used to obtain W_n and ω_{ex}. The overdetermined system of six linear equations with only two unknowns can be solved using linear least squares methods [58]. In our case, a simple Matlab program was written to automatically determine optimum values of W_n and ω_{ex}. The listing of the program for T=292 K and the value of mixing time T_m=500 ns is shown in the Appendix section.

The output of the program is two parameters *b* and *c* which can be directly transformed to the relaxation rates W_n and ω_{ex} by means of the equations (20), (21) for each value of the mixing time T_m. The values of W_n and ω_{ex} as well as parameters *b* and *c* for five mixing times and temperature T=292 K are presented in Table 2.

Table 2 Parameters b, c, W_n and ω_{ex} for a series of 2D-ELDOR spectra (T=292 K)

Mixing Time	***b***	***c***	***2W$_n$***	***ω_{ex}***
200	0.7026	0.6973	1.893E+04	1.746E+06
300	0.6494	0.5772	1.964E+05	1.243E+06
500	0.5031	0.3957	2.401E+05	1.134E+06
1000	0.28	0.1592	2.823E+05	9.907E+05
2000	0.1553	0.0963	1.195E+05	8.117E+05
Average			1.7E+05	1.2E+06

As mentioned in Chapter 2.2.4, the collision frequency is $\nu_{coll} = 3 \cdot \omega_{ex}$. Taking the average value of ω_{ex} from the table above, we get ν_{coll}=3.6·10^{-6} s^{-1}. Error was estimated to be around 15 %.

In order to calculate diffusion coefficient D, we can employ the method developed by Devaux and co-workers [59]. Here, the diffusion is considered as a nearest-neighbour exchange on a lattice. To be exact, each lipid molecule is assumed to be at the center of a hexagon, having six surrounding molecules. Thus, a given lipid molecule encounters three new nearest molecules while keeping the contact with three previous molecules. In this case, the collision frequency of spin labels can be estimated by

$$\nu_{coll} = 3 \cdot \nu \cdot c \tag{23}$$

where ν is a hopping frequency between adjacent lattice sites, and c is a mole fraction of a spin label. Parameter ν can be eliminated by using the Einstein formula for the two-dimensional diffusion

$$D = \tfrac{1}{4} \nu \lambda^2 \tag{24}$$

where λ is the lattice spacing (or alternatively the length of one jump).

Then, after combining equations (23) and (24) and assuming that D should be replaced with $2 \cdot D$ for bimolecular diffusive encounters [60],

$$D = \left(\frac{\lambda^2}{24} \right) \left(\frac{\nu_{coll}}{c} \right) \tag{25}$$

Using equation (25) and assuming that λ is equal to 8 Å [9], we can estimate $D = 2.4 \cdot 10^{-8}$ sm^2s^{-1} which appear to be reasonable value for system under investigation.

4.0 SUMMARY AND CONCLUSIONS

This thesis has focused on the problem of quantifying lateral diffusion of the lipids in a membrane. Different methods to obtain diffusion coefficient *D* were discussed. The long range diffusion measurements were presented by Fluorescence Recovery after Photobleaching (FRAP) method. The short-range diffusion measurements were presented by variants of fluorescence spectroscopy methods as well as NMR and ESR spectroscopy approaches. Relative merits and disadvantages of each technique were compared. Special attention was given to the ESR spectroscopy method including general discussion about sensitivity to rotational and translational motion as well as effects that contribute to the shape of ESR spectrum.

Novel two-dimensional Fourier Transform ESR approach has been reviewed. Advantages of this method with comparison to the conventional continuous wave ESR spectroscopy were mentioned. Two dimensional electron-electron double resonance experiment (2D-ELDOR) is the technique that provides information about translational motion through measurements of Heisenberg spin Exchange rates. Quantitative estimates of HE can be obtained by comparing experimental data with spectral simulations based on the Stochastic Liouville equations. Another way to extract HE rates from 2D plots is to extract peak volumes and solve overdetermined system of six linear equations. In general, this leads to the values of ^{14}N nuclear relaxation rate W_n and Heisenberg exchange frequency ω_{ex}. HE frequency can be directly related to collision frequency and to the diffusion coefficient *D* by considering theoretical model for diffusion process.

In order to demonstrate the whole procedure of extracting translational rates using 2D-ELDOR experiment, a series of experiments was performed on the sample of phospholipids mixed with a spin label (DphPC and perdeuterated tempone). The value of diffusion coefficient D is in the good agreement with literature values and has an order of $\sim 10^{-8}$ cm^2s^{-1}.

APPENDIX

THE LISTING OF THE MATLAB PROGRAM

```
% Program for calculating b and c parameters for overdetrmined system Ax=d (2D-Eldor case)
% The overdetermined system (more equations than unknowns) is solved using the Matlab command \
% which automatically finds the solution that minimizes the squared error in Ax-d.
%  This solution is called the least square solution.
A = [
 0                    1.3297;
 0                    1.1863;
 0.2626               1.0875;
 0.4561               1.152;
 0.5781               -0.1027;
 0.3975               -0.0844
 ];

d = [
 0.6643;
 0.3826;
 0.8249;
 0.696;
 0.2053;
 0.1687
 ];

x = A \ d % the column-oriented solution of a linear system

dif = A*x - d   % check that the solution x is correct
```

BIBLIOGRAPHY

1. Tocanne, J.-F., Dupou-Cezanne, L. and Lopez, A., *Lateral diffusion of lipids in model and natural membranes.* Prog. Lipid Res., 1994. **33**(3): p. 203-237.

2. Singer, S.J., Nicholson, G.I., *The fluid mosaic model of cell membranes.* Science, 1972. **175**: p. 720-731.

3. *http://www.bmb.psu.edu/courses/bisci004a/cells/cellstruc.htm*.

4. Stryer, L., *Biochemistry*. 4th ed. 1995, New York: W.H. Freeman. xxxiv, 1064.

5. Venable, R.M., Zhang Y., Hardy B.J., Pastor R.W., Science, 1993. **262**: p. 223-226.

6. Haines, T.H., FEBS Lett., 1994. **346**: p. 115-122.

7. Gorcester, J., Freed, J.H., J. Chem. Phys., 1988. **88**: p. 4678-4693.

8. Bowman, M.K. and L. Kevan, *Modern pulsed and continuous-wave electron spin resonance*. 1990, New York: Wiley. ix, 440 p.

9. Grell, E., *Membrane spectroscopy*. Molecular biology, biochemistry, and biophysics ; 31. 1981, Berlin ; New York: Springer-Verlag. xi, 498.

10. Becker, R.S., *Theory and interpretation of fluorescence and phosphorescence*. 1969, New York,: Wiley Interscience. xiv, 283 p.,.

11. Parker, C.A., *Photoluminescence of solutions. With applications to photochemistry and analytical chemistry*. 1968, Amsterdam, New York [etc.]: Elsevier Pub. Co. xvi, 544 p.

12. Poste, G. and G.L. Nicolson, *Membrane reconstitution*. Cell surface reviews ; v. 8. 1982: North-Holland Pub. Co. 83-136.

13. Elson, E.L., *Membrane dynamics studied by fluorescence correlation spectroscopy and photobleaching recovery.* Soc. Gen. Physiol. Ser., 1986. **40**: p. 367-383.

14. Yguerabide, J., Biophys. Soc. Annu. Meet. Abstr., 1971.

15. Poo, M., Cone, R.A., Nature, 1974. **247**: p. 438-441.

16. Axelrod, D., Koppel, D.E., Schlessinger, J., Elson, E. and Webb, W.W., Biophys. J., 1976. **16**: p. 1055-1069.

17. Soucaille, P., Prats, M., Tocanne, J.F. and Teissie, J., Biochim. Biophys. Acta, 1988. **939**: p. 289-294.

18. Chattopadhyay, A., London, E., Biochemistry, 1987. **26**: p. 39-45.

19. Wu, E.S., Jacosson, K., Papahadjoulos, D., Biochemistry, 1977. **16**: p. 3936-3941.

20. Golan, D.E., Alecio, M. R., Veatch, W. R., Rando, R. R., Biochemistry, 1984. **23**: p. 332-339.

21. Rubenstein, J.L.R., Smith, B. A., Mcconnell, H. M., Proc. Natl. Acad. Sci. U.S.A., 1979. **76**: p. 15-18.

22. Alecio, M.R., Golan, D.E.Veatch, W. R., Rando, R. R.,, Proc. Natl. Acad. Sci. U.S.A., 1982. **79**: p. 5171-5174.

23. Kapitza, H.G., Ruppel, D. A., Galla, H. J., Sackmann, E., Biophys. J., 1984. **45**: p. 577-587.

24. Fato, R., Battino, M., Parenti-Castelli, G. and Lenaz, G., FEBS Lett., 1985. **179**: p. 238-242.

25. Fato, R., Battino, M., Degli Esposti, M., Parenti-Castelli, G. and Lenaz, G., Biochemistry, 1986. **25**: p. 3378-3390.

26. Owen, C.S., J. Chem. Phys., 1975. **62**: p. 3204-3207.

27. Blackwell, M.F., Gounaris, K., Zara, S.J. and Barber, J., Biophys. J., 1987. **51**: p. 735-744.

28. Caruso, F., Grieser, F., Murphy, A., Thistlethwaite, P., Urquhart, R., Almgren, M. and Wistus, E., J. Am. Chem. Soc., 1991. **113**: p. 4838-4843.

29. Caruso, F., Thistlethwaite, P., Grieser, F., The ACS Journal of Surfaces and Colloids, 1994. **10**(10): p. 3373-3376.

30. Stryer, L., Thomas, D.D. and Meares, C.F., Annu. Rev. Biophys. Bioeng., 1982. **11**: p. 203-222.

31. Thomas, D.D., Carlsen, W.F., Stryer, L., Proc. Natl. Acad. Sci. U.S.A., 1979. **75**: p. 5746-5750.

32. Callaghan, P.T., *Principles of nuclear magnetic resonance microscopy*. 1991: Clarendon Press ;
Oxford University Press. xvii, 492 p.

33. Lindblom, G., Oradd, G., Prog. Nucl. Magn. Reson. Spectrosc., 1994. **26**: p. 483-515.

34. Stilbs, P., Prog. Nucl. Magn. Reson. Spectrosc., 1987. **19**: p. 1-45.

35. Stejscal, E.O., Tanner J.E., J. Chem. Phys., 1965. **42**: p. 288.

36. Oradd, G., Lindblom, G., Magn. Reson. Chem., 2004. **42**: p. 123-131.

37. Tanner, J.E., J. Chem. Phys., 1970. **52**: p. 2523.

38. Lahajnar, G., Zupancic, I., Period. Biol., 1981. **83**: p. 159-162.

39. Crawford, M.S., Gerstein, B.C., Kuo, A.L. and Wade, C.G., J. Am. Chem. Soc., 1980. **102**: p. 3728-3732.

40. Cullis, P.R., FEBS Lett., 1976. **70**: p. 223-228.

41. Weil, J.A., J.R. Bolton, and J.E. Wertz, *Electron paramagnetic resonance : elementary theory and practical applications*. 1994, New York: Wiley. xxi, 568 p.

42. Crepeau, R.H., Saxena S.K., Lee, S., Patyal, B., Freed J.H., Biophys. J., 1994. **66**: p. 1489-1504.

43. Meirovitch, E., Nayeem, A., Freed J.H., J. Phys. Chem., 1984. **88**: p. 3454-3465.

44. Borbat, P.P., Costa-Filho, A.J., Earle, K.A., Moscicki, J.K., Freed, J.H., Science, 2001. **291**: p. 266.

45. Schweiger, A. and G. Jeschke, *Principles of pulse electron paramagnetic resonance*. 2001, Oxford, UK ; New York: Oxford University Press. xxvi, 578 p.

46. Berliner, L.J. and J. Reuben, *Spin labeling : theory and applications*. Biological magnetic resonance, v. 8. 1989, New York ; London: Plenum. xix, 650.

47. Trauble, H., Sackman, E., J. Am. Chem. Soc., 1972. **94**: p. 4499-4510.

48. Stuart, R., Marshall, W, Phys. Rev., 1960. **120**: p. 353.

49. Devaux, P., McConnell, H., J. Am. Chem. Soc., 1972. **94**: p. 4475-4481.

50. Popp, C.A., Hyde, J.S., Proc. Natl. Acad. Sci. U.S.A., 1982. **79**: p. 2559-2563.

51. Feix, J.B., Popp, C.A., Venkataramu, S.D., Beth, A.H., Park, J.H. and Hyde, J.S., Biochemistry, 1984. **23**: p. 2293-2299.

52. Yin, J.J., Pasenkiewich-Gierula, M. and Hyde, J.S., Proc. Natl. Acad. Sci. U.S.A., 1987. **84**: p. 964-968.

53. Miick, S.M., Millhauser G.L., J. Magn. Reson., 1994. **104**: p. 81-84.

54. Borbat, P.P., Crepeau R.H., Freed, J.H., J. Magn. Reson., 1997. **127**: p. 155.

55. Bonora, M., Pornsuwan, S., Saxena, S., J. Phys. Chem. B, 2004. **108**: p. 4196-4198.

56. Gorcester, J., Rananavare S.,B., Freed, J.H., J. Chem. Phys., 1989. **90**: p. 5764-5786.

57. Kevan, L. and M.K. Bowman, *Modern pulsed and continuous-wave electron spin resonance*. 1990, New York ; Chichester: Wiley. 119-194.

58. Press, W.H., *Numerical recipes : the art of scientific computing*. 1986, Cambridge [Cambridgeshire] ; New York: Cambridge University Press. xx, 818 p.

59. Devaux, P.F., Scandella, C.J., McConnell, H.M., J. Magn. Reson., 1973. **9**: p. 474-485.

60. Sachse, J.H., King, M.D., Marsh D., J. Magn. Reson., 1987. **71**: p. 385-404.